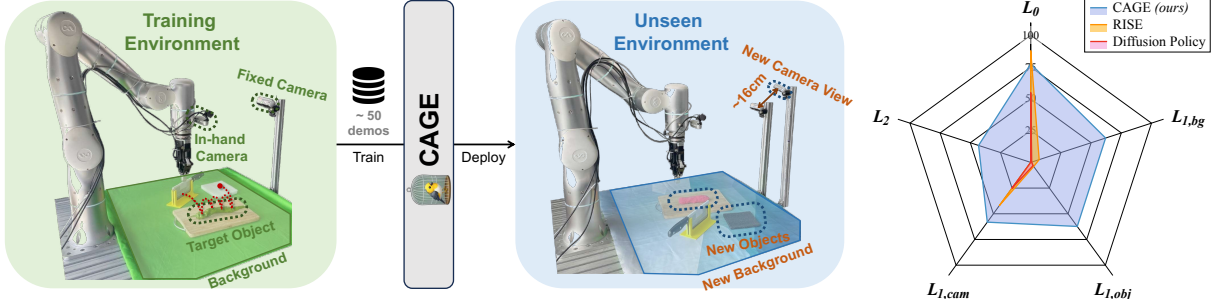


# CAGE: Causal Attention Enables Data-Efficient Generalizable Robotic Manipulation

Shangning Xia<sup>1</sup>, Hongjie Fang<sup>1,2</sup>, Cewu Lu<sup>1,2,†</sup>, Hao-Shu Fang<sup>1,†</sup>



**Fig. 1:** CAGE is a data-efficient generalizable robotic manipulation policy. With approximately 50 mono-distributed demonstrations, CAGE can effectively complete the task in test environments with different levels of distribution shifts (See §IV-A.6 for details): training environment ( $L_0$ ), similar environment ( $L_1$ ), and unseen environment ( $L_2$ ). Experiments demonstrate that CAGE generalizes well to  $L_1$  and  $L_2$  environments and significantly outperforms prior works.

**Abstract**—Generalization in robotic manipulation remains a critical challenge, particularly when scaling to new environments with limited demonstrations. This paper introduces CAGE, a novel robotic manipulation policy designed to overcome these generalization barriers by integrating a causal attention mechanism. CAGE utilizes the powerful feature extraction capabilities of the vision foundation model DINOv2, combined with LoRA fine-tuning for robust environment understanding. The policy further employs a causal Perceiver for effective token compression and a diffusion-based action prediction head with attention mechanisms to enhance task-specific fine-grained conditioning. With as few as 50 demonstrations from a single training environment, CAGE achieves robust generalization across diverse visual changes in objects, backgrounds, and viewpoints. Extensive experiments validate that CAGE significantly outperforms existing state-of-the-art RGB/RGB-D approaches in various manipulation tasks, especially under large distribution shifts. In similar environments, CAGE offers an average of 42% increase in task completion rate. While all baselines fail to execute the task in unseen environments, CAGE manages to obtain a 43% completion rate and a 51% success rate in average, making a huge step towards practical deployment of robots in real-world settings. Project website: [cage-policy.github.io](https://cage-policy.github.io).

## I. INTRODUCTION

Generalization is one of the ultimate goals of robotic manipulation. Despite progress in certain areas like general grasping [13, 52], broader manipulation tasks still require significant development. Recent advances in imitation learning [2, 6, 54, 59] highlight the potential of behavior-cloning-based [40] robotic manipulation policies in learning from demonstrations. However, behavior cloning often struggles with out-of-distribution scenarios, leading to compounded

errors and task failures, which emphasizes the importance of generalization ability in the robotic manipulation policy.

Aiming at a generalizable robotic manipulation policy, previous research has concentrated on two main directions: (1) collecting or creating more demonstration data for policy training, and (2) searching for a better representation of environment perceptions for robotic manipulation tasks.

For the former direction, several studies have collected large-scale robotic datasets [2, 14, 27, 8, 51] and trained robotic foundation models on those datasets. While these solutions do show an improved generalization performance in evaluations, a fundamental question remains: *Does the policy itself truly generalize, or is the superior performance attributable to the policy having seen similar demonstrations during training?*

We believe that the upper limit of a policy’s generalization ability is determined by its inherent structure, and merely increasing the amount of training data can only narrow the gap instead of elevating the limit. Therefore, we opt for the second path to *address the generalization issue at its core*. Many studies [17, 54, 55, 58] directly perceive the point cloud observations to produce a generalizable 3D scene-level representation for downstream control policy, effectively generalizing across different camera views through calibrations [54]. However, unlike the success of visual foundation models (VFM) [5, 37, 42] in images, the lack of generic pre-trained foundation models for 3D point clouds can limit the generalization capabilities of these methods at the object level, especially when facing objects with completely different geometries.

Alternatively, some literature [32, 33, 35, 43, 47] proposes decoupling perception and control in the policy by using pre-trained 2D visual representations for manipulations, but they offer limited advantages over VFM in generalization evaluations [3]. SOFT [41] investigates the use of interme-

<sup>1</sup> Shanghai Jiao Tong University.

<sup>2</sup> Shanghai Artificial Intelligence Laboratory.

† Cewu Lu and Hao-Shu Fang are the corresponding authors.  
 {ritchie\_xia, galaxies, lucewu}@sjtu.edu.cn, fhaoshu@gmail.com.

diate features from VFM and achieves competitive results against manipulation-specific pre-training, underscoring the capability of VFM to enhance robot control policies in environmental perception with their extensive and diverse knowledge acquired from large-scale pre-training.

To this end, we introduce CAGE, a data-efficient and generalizable robotic manipulation policy enabled by causal attention. With approximately 50 demonstrations from a single training environment, CAGE can sustain its performance in test environments with unseen objects, backgrounds, and camera views. CAGE integrates DINOv2 [37] with LoRA [23] fine-tuning to perceive image observations, efficiently extracts manipulation-relevant features from raw observation tokens via the causal perceiver, and employs fine-grained attention-based conditioning to apply these features within the control policy. Extensive experiments demonstrate that CAGE can effectively generalize across different levels of distribution shifts, and outperforms prior methods by a large margin.

## II. RELATED WORKS

### A. Generalizable Robotic Manipulation

Current generalist robotic manipulation policies [1, 2, 8, 28, 48, 36, 56, 57, 60] are mainly trained under a multi-task setting using extensive robot demonstration data [1, 2, 8, 48], and generalization in these policies is predominantly discussed in the context of unseen tasks. Given the multi-task training setup and large volumes of data, it can be straightforward to find similar task combinations within the training data that may resemble the “unseen” tasks. As a result, as previously discussed in §I, it is challenging to determine whether the policy truly generalizes.

Therefore, we focus on a single-task setup and elevate the task to an abstract skill, making it adaptable to different target objects. While 2D image-based policies Diffusion Policy (DP) [6] and ACT [59] perform well during in-domain evaluations, their generalization abilities are limited to minor environmental variations. In contrast, 3D point-cloud-based policies [54, 55] can naturally handle spatial generalization across camera views, so long as the cameras are well-calibrated. Among these policies, RISE [54] thoroughly evaluates its generalization ability in the real world and demonstrates state-of-the-art generalization performance across various environmental disturbances.

In this paper, we meticulously design experiments to assess the generalization performance of robotic manipulation policies. The highest level of generalization corresponds to testing in an entirely unseen environment, which rigorously evaluates the true generalization capability of the policy.

### B. Visual Representation Learning for Manipulation

Visual representation learning for manipulation primarily aims to generate useful and meaningful representations of current observation images, which are then used as inputs for control policies.

One line of methods decouples visual representation learning from the control policy. Some [32, 33, 35, 43] focus on

pre-training vision encoders [12, 21] on large-scale human manipulation datasets [10, 18, 19, 46] using self-supervision schemes [20, 22] for manipulation policies. However, recent studies [3, 41] show that generic pre-trained VFM [29, 37, 42] can achieve comparable or even better generalization performance than these pre-trained visual representations. Others investigate directly using VFM representations [3, 11, 41] or distilling VFM representations [47] for downstream learning, but it may overlook task-specific features in visually complex tasks without the fine-tuning process. VINN [38] first trains visual representations from scratch using the demonstration dataset, and subsequently uses these representations to retrieve actions from the dataset, but its generalization capability is limited due to representation learning being restricted to the demonstration dataset domain.

Another line of research trains the visual encoder and the control policy together in an end-to-end manner. Some initialize pre-trained weights to the visual encoder for generalization considerations [7, 36]. SpawnNet [30] designs adapter layers to integrate intermediate representations from both the encoder and a pre-trained encoder, enhancing generalization performance, but the large number of trainable parameters poses challenges in applying it to VFM.

Inspired by recent advances in parameter-efficient fine-tuning of foundation models, we apply LoRA [23] for fine-tuning the VFM (DINOv2 [37]) to enhance observation perception effectively. Perhaps the most similar to our work is SAM-E [57], which also leverages the VFM (SAM [29]) with LoRA fine-tuning for image perception. Nonetheless, as demonstrated in §IV-E, naively substituting visual encoders with VFM yields limited generalization improvements, underscoring the effectiveness of our entire policy architecture.

## III. METHOD

At current timestep  $t$ , with the observation horizon  $T_o$ , the robot receives stacks of images  $I_t \in \mathbb{R}^{N_c \times T_o \times H \times W \times 3}$  from  $N_c$  RGB cameras and proprioceptions  $p_t \in \mathbb{R}^{T_o \times D_p}$  within the latest  $T_o$  horizon, where  $H \times W$  is the image size and  $D_p$  is the proprioception dimension. Our CAGE policy  $f_\phi$  with parameters  $\phi$  takes  $I_t$  and  $p_t$  as inputs and generate a continuous action sequence  $a_t$  starting from  $t$ , with action horizon  $T_a$ , *i.e.*,

$$a_t = f_\phi(I_t, p_t) \in \mathbb{R}^{T_a \times D_a}, \quad (1)$$

where  $D_a$  is the action dimension. Beyond learning from collected demonstrations, *generalizing to similar and unseen environments* is also essential for robust robotic manipulation policies, especially in the real world.

Due to the promising performance of DP [6] in robotic manipulations, we build our CAGE upon it, incorporating 3 key design components for better generalization capability: DINOv2 [37] image encoder with LoRA [23] fine-tuning (§III-A), causal perceiver for token compression (§III-B), and UNet diffusion action head with attention for effective conditioning (§III-C). Experiments show that all three parts are critical for the overall generalization ability. The architecture of CAGE is shown in Fig. 2.

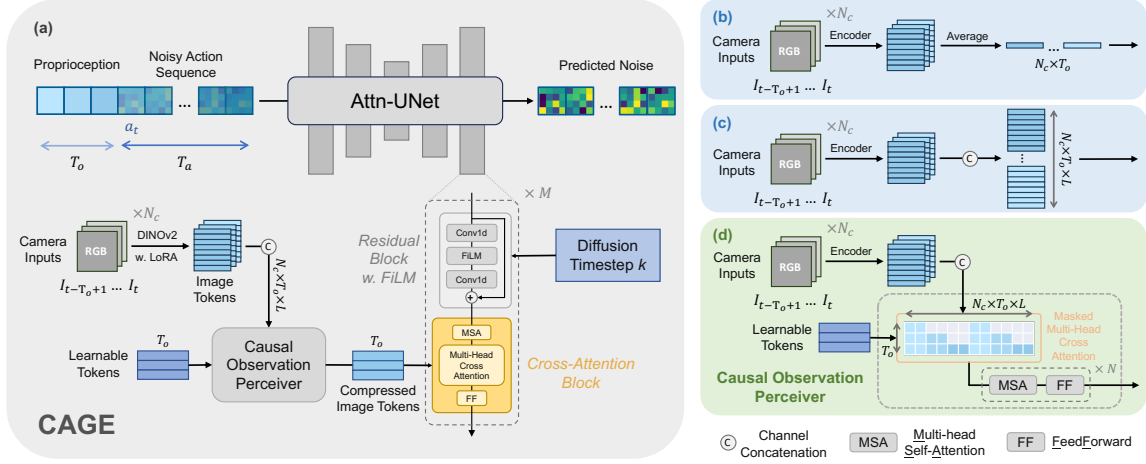


**Fig. 2: (a) Overview of CAGE.** CAGE is composed of three parts: 1) observation images are passed to DINOv2 image encoder (LoRA fine-tuning) to obtain observation tokens. 2) The concatenated observation tokens are compressed by *Causal Observation Perceiver*. The learned tokens, along with the timestep embeddings serve as the conditioning for noise prediction. 3) The Attn-UNet takes as input a sequence of noisy actions prefixed by proprioceptions and outputs noise estimation, following standard diffusion procedure. **(b) Averaging over tokens for compression** loses critical scene-level positional information. **(c) Directly using as downstream inputs** is inefficient due to the large number of tokens. **(d) Our proposed *Causal Observation Perceiver* for token compression.**

### A. Visual Foundation Model as Image Encoder

Most prior studies [1, 2, 6, 34, 59] prefer to utilize a lightweight CNN as the observation encoder for images, with these encoders typically being trained from scratch. This approach, while computationally efficient, has been found to result in rapid overfitting to the image domain of the training environment, restricting the generalization ability of the policy to even moderate visual variations that deviate from the training data. Recently, researchers have been investigating the use of ViT [12] as image encoders to enhance policy performance [7, 31], but naively training ViT from scratch has shown limited improvement in the generalization capabilities of the policy.

In pursuit of a generalizable robotic manipulation policy, we utilize the VFM DINOv2 [37] (denoted as  $h_\psi$  with parameters  $\psi$ ) as our vision backbone due to its ability to extract rich and semantically meaningful features for downstream visual tasks. Unlike prior approaches that directly use DINOv2 features for downstream learning [3, 11, 41], we adopt a different strategy by keeping the pre-trained weights  $\psi^*$  of DINOv2 frozen and employing LoRA [23] for parameter-efficient fine-tuning with additional tuning parameters  $\psi_{\text{LoRA}}$ . This approach allows us to maintain the emergent segmentation capabilities of DINOv2 in out-of-distribution environments [3, 4], while simultaneously adapting it for robotic manipulations to extract more task-relevant features. Specifically, our DINOv2 image encoder produces the following tokens

$$E_t = h_{\psi^* + \psi_{\text{LoRA}}}(I_t) \in \mathbb{R}^{(N_c \times T_o \times L) \times D_{\text{token}}}, \quad (2)$$

where  $L$  is the number of tokens in a single input image,  $D_{\text{token}}$  is the token dimension.

### B. Causal Perceiver for Token Compression

After processing the image observations via the encoder, we obtain  $N_c \times T_o \times L$  image tokens in  $E_t$ . Common practices

for handling such image tokens include averaging over them (Fig. 2(b)) [3, 34, 41], or using the entire token sequence as input (Fig. 2(c)) [1, 2, 36, 59, 60]. Yet, both methods present challenges in our context. Averaging loses critical scene-level positional information while using the entire token sequence is inefficient due to the large number of tokens.

Inspired by [48, 53], we propose a causal PerceiverIO-like [26] structure (denoted as  $g_\xi$  with parameters  $\xi$ ) to efficiently compress the image tokens and extract the most relevant features for manipulation from the image tokens  $E_t$ . The  $N_c \times T_o \times L$  image tokens from  $N_c$  cameras within the observation horizon  $T_o$  are first cross-attended by  $T_o$  learnable tokens to compress into  $T_o$  tokens within the observation horizon, with causal attention mask shown in Fig. 2(d). Then the output tokens are fed into  $N$  causal transformer blocks to further process the extracted information. Formally, the causal perceiver  $g_\xi$  compresses  $N_c \times T_o \times L$  image tokens  $E_t$  into  $T_o$  tokens  $E_t^*$ , with

$$E_t^* = g_\xi(E_t) \in \mathbb{R}^{T_o \times D_{\text{token}}}. \quad (3)$$

In this way, the compressed tokens  $E_t^*$  can effectively retain both spatial and temporal information, which are equally important for manipulation tasks.

### C. Diffusion Action Head with Attention

The original UNet-based [45] diffusion action head [6] employs FiLM [39] conditioning mechanics for the observation inputs. However, the FiLM module is non-expandable as it only accepts 1D input, limiting the expressivity of the observation conditions. Simply flattening the compressed tokens into one dimension will ignore the temporal relationship among  $T_o$  compressed tokens in the observation horizon.

To mitigate this issue, we propose to decouple the conditioning of diffusion step  $k$  and compressed image tokens  $E_t^*$ . By employing a structure that incorporates a residual block [21] followed by a cross-attention block [50], which is

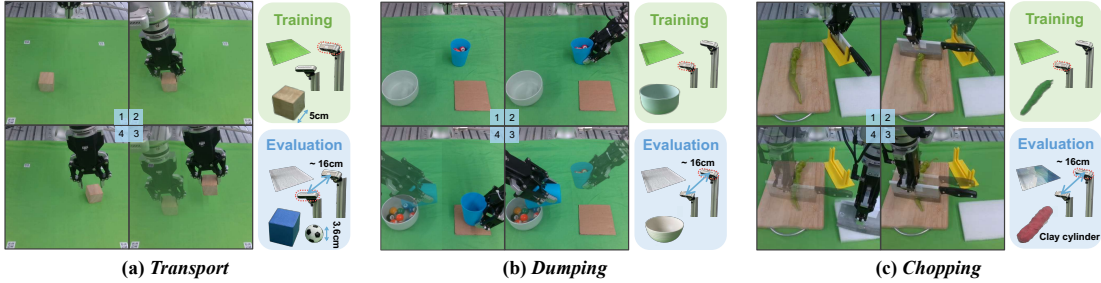


**Fig. 3: Tasks with Generalization Variations.** (a) **Transport**: the robot needs to localize the object on the left side of the workspace (*reach*), grasp it (*grasp*), and drop it to the right side (*drop*). (b) **Dumping**: the robot needs to grasp the cup horizontally (*grasp*), move it over the bowl, tilt it until all balls are out into the bowl (*pour*), and place the cup in the target area (*place*). (c) **Chopping**: the robot needs to grasp the kitchen knife (*grasp*), use the knife to chop the object<sup>1</sup> on the cutting board into several pieces (*chop*), and place the knife safely on the foam pad (*place*). **Generalization variations** include different backgrounds, objects, and camera views (please refer to §IV-A.6 for detailed explanations).

similar to the 2D UNet backbone in Stable Diffusion [44], we can apply diffusion step  $k$  conditioning in the residual block via FiLM [39] and use cross-attention to condition on the compressed image tokens  $E_t^*$ . FiLM offers efficient global conditioning with the diffusion step, while cross-attention enables fine-grained conditioning with image tokens.

The UNet-based diffusion action head (denoted as  $\epsilon_\varphi$  with parameters  $\varphi$ ) is modified accordingly, as illustrated in Fig. 2, which we refer to as *Attn-UNet*. The action is then iteratively denoised using the DDIM [49] schedule.

$$a_t^{(k-1)} = \alpha_k a_t^{(k)} - \beta_k \epsilon_\varphi \left( a_t^{(k)}; E_t^*, k \right) \in \mathbb{R}^{T_a \times D_a}, \quad (4)$$

where  $k$  is the diffusion step,  $\{\alpha_k, \beta_k\}$  is the noise schedule, and  $a_t = a_t^{(0)}$  is the generated continuous action trajectory.

In summary, CAGE is parameterized by the combination of the trainable parameters in each module, with a frozen DINOv2 weights  $\psi^*$ , *i.e.*,  $\phi = (\psi_{\text{LoRA}}, \xi, \varphi; \psi^*)$ .

## IV. EXPERIMENTS

### A. Setup

1) *Platform*: We employ a Flexiv Rizon robotic arm [15] with a Dahuan AG-95 gripper [9] as our robot platform. A rectangle area of 45cm  $\times$  60cm in the center of the tabletop is selected as the robot workspace. We adopt a binocular vision setting with 2 Intel RealSense D435 cameras [25]: one fixed camera in front of the robot facing towards the workspace, and one in-hand camera above the gripper on the end of the robotic arm.

2) *Baselines*: We choose the 2D image-based Diffusion Policy (DP) [6], and the current state-of-the-art 3D point-cloud-based policy RISE [54] with decent generalization performance in the real world as baselines. For DP, RGB images from both cameras are used, whereas the RGB-D frames from only the fixed camera are provided to RISE following its original implementation. Both methods are trained from scratch with their recommended hyper-parameter settings. Please refer to Appendix A for details.

<sup>1</sup>We use real peppers during data collection. However, to avoid unnecessary waste, we make a pepper out of clay for evaluation.

3) *Tasks*: In order to provide a comprehensive coverage of robotic manipulation problems, we design 3 tasks with *generalizable skills* (illustrated in Fig. 3), each focusing on a different aspect of robotic manipulation: **Transport** (Pick-and-Place), **Dumping** (6-Dof) and **Chopping** (Long horizon). With a special focus on generalization, our tasks are designed at the skill level, so we do not impose strict requirements on the objects, and they can be substituted with any similar items during evaluations.

4) *Demonstrations*: Following [14], human-teleoperated demonstrations are collected via a haptic device [16]. We collect 50 demonstrations for the **Transport** task, and 40 demonstrations for the **Dumping** and the **Chopping** tasks each. To properly assess the real generalization capabilities of each policy, the variations of background, object, and camera view are deliberately limited in demonstrations for a more restricted training environment.

5) *Evaluation Protocols*: Evaluations are conducted on a workstation with an Intel Core i9-10900K CPU and an NVIDIA RTX 3090 GPU linked to the robot platform. During the evaluation, we run the inference process and the execution process in parallel for continuous control with a frequency of 10Hz. During the evaluations, we randomly and uniformly generate test positions beforehand for each task and initialize the workspace accordingly, ensuring a fair, consistent, and reproducible comparison across different methods. We report stage-wise success rates (the stages are defined in the caption of Fig. 3) to evaluate the performance throughout the task. For the **Dumping** and the **Chopping** tasks, we also report the task completion rates, including the average number of balls poured into the bowl (# ball), the average number of poured balls if successfully grasped (# ball (g)), and the average number of chops (# chop) respectively.

6) *Generalization Levels*: We meticulously devised 3 levels of tests to evaluate thoroughly each policy’s generalization capabilities:

- **L<sub>0</sub> generalization** refers to evaluations in the *training environment* with the same background, seen objects, and the same camera view;
- **L<sub>1</sub> generalization** refers to evaluations in a *similar environment* with the variation in one of the three

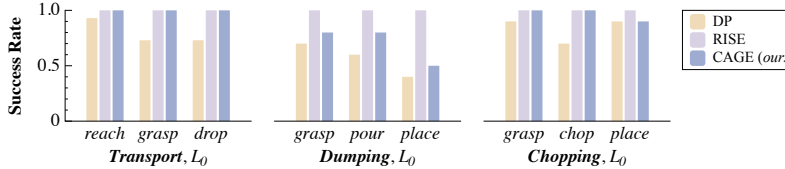


**TABLE I: Results of the  $L_0$  Evaluation.** The  $L_0$  evaluation is conducted in the same environments seen during training. CAGE outperforms DP in all tasks, and performs comparably with RISE in most tasks.

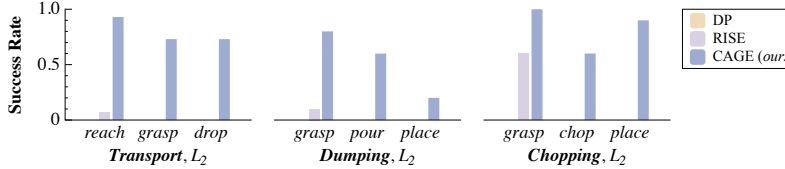


**TABLE II: Results of the  $L_2$  Evaluation.** The  $L_2$  evaluation is conducted in unseen environments, with different backgrounds, camera views and unseen objects. CAGE largely outperforms all baselines in all tasks.

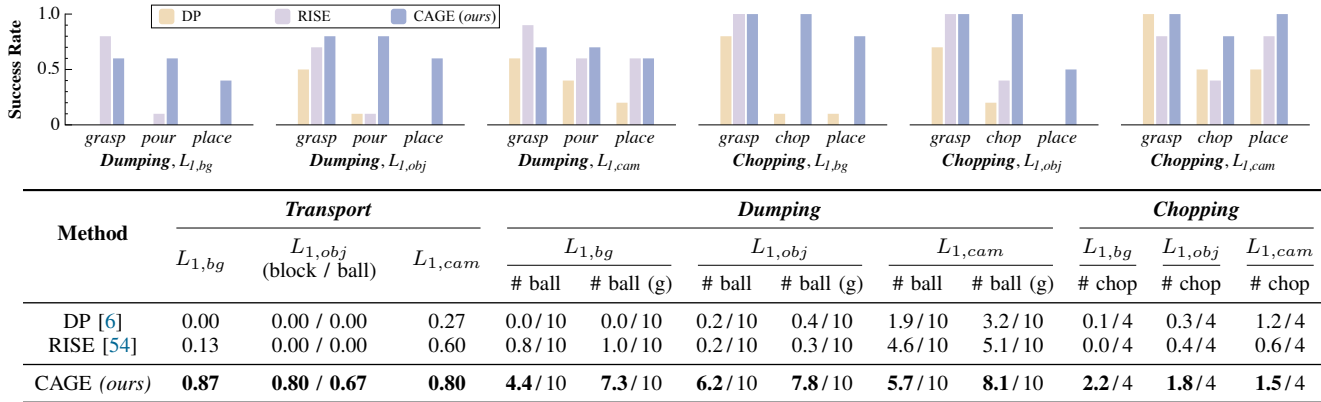


**TABLE III: Results of the  $L_1$  Evaluation.** The  $L_1$  evaluation is conducted in similar environments, with one of the variations in backgrounds, objects and camera views. The overall success rates are reported for the **Transport** task here. CAGE surpasses RISE on success rates and completion rates across all tasks.

aforementioned aspects, denoted as  $L_{1,bg}$ ,  $L_{1,obj}$  and  $L_{1,cam}$  respectively;

- **$L_2$  generalization** refers to evaluations in an *unseen environment* with variations present across all three aspects, thereby emulating the scenario in real-world deployment.

7) *Implementations*: For each task, CAGE is trained with a batch size of 64 on 4 NVIDIA A100 80GB GPUs for 500 epochs. We set  $N_c = 2$  based on the binocular vision settings in our robot platform. For the vision encoder, we choose DINOv2-large [37] as the backbone and set the LoRA [23] rank to 16. We set the observation horizon  $T_o = 4$  and the action horizon  $T_a = 20$  with a relative action representation [7]. Unlike prior works [6, 7, 59], the data preprocessings are limited to color jitter and center crop to ensure a out-of-distribution evaluation of camera viewpoint generalization. However, we conduct experiments with additional geometric augmentations to show the full potential of CAGE in §IV-E.

## B. Results

1) *Training Environment*: For the  $L_0$  evaluations in the same environment, we present the results in Tab. I.

Method / Task	<i>Dumping</i>		<i>Chopping</i>
	# ball	# ball (g)	# chop
DP [6]	4.2/10	7.0/10	2.0/4
RISE [54]	<b>9.3</b> /10	9.3/10	<b>2.8</b> /4
CAGE (ours)	7.5/10	<b>9.4</b> /10	2.3/4

Method / Task	<i>Dumping</i>		<i>Chopping</i>
	# ball	# ball (g)	# chop
DP [6]	0.0/10	0.0/10	0.0/4
RISE [54]	0.0/10	0.0/10	0.0/4
CAGE (ours)	<b>3.4</b> /10	<b>5.7</b> /10	<b>0.9</b> /4

**CAGE consistently outperforms DP and performs comparably to RISE in most tasks under in-domain environments.** In the training environment, CAGE surpasses DP in all tasks. RISE, which utilizes 3D point cloud information, generally performs the best among all methods. However, CAGE still shows comparable performance to RISE in the **Transport** and the **Chopping** tasks. For the **Dumping** task, precise cup localization is critical to avoid task failure due to collisions, and 2D image-based policy CAGE are naturally less accurate in position prediction than 3D point-cloud-based policy RISE. But if we only consider the average number of balls poured over successful grasps, CAGE actually performs the pouring action slightly better than RISE.

2) *Similar Environment*: For the visually altered  $L_1$  evaluations, we design several challenging environments such as replacing the block with a ball of drastic differences in both size and geometry for the **Transport** task. The results are shown in Tab. III.

**CAGE demonstrates effective generalization across various similar environments, with an acceptable performance decline in general.** While subtle visual changes in the evaluation environments challenge both DP and RISE, pre-

Platform		Transport, similar			Dumping, similar				
Robot	Gripper	reach	grasp	drop	grasp	pour	place	# ball	# ball (g)
Flexiv	Dahuan	1.00	1.00	1.00	0.80	0.80	0.50	7.5/10	9.4/10
Flexiv	Robotiq	0.73	0.60	0.60	0.40	0.40	0.40	3.2/10	8.0/10
RealMan	Dahuan	0.53	0.47	0.47	0.20	0.20	0.10	1.2/10	6.0/10

**TABLE IV: Cross-Embodiment Evaluation Results under *Similar* Environment.** *Similar* denotes a similar environment setup with a green background, the same objects, and a close camera view. The background and the camera are not identical to the training environment as their platforms are different. New hardware is highlighted in yellow.

Platform		Transport, novel			Dumping, novel				
Robot	Gripper	reach	grasp	drop	grasp	pour	place	# ball	# ball (g)
Flexiv	Dahuan	0.93	0.73	0.73	0.80	0.60	0.20	3.4/10	4.3/10
Flexiv	Robotiq	0.60	0.53	0.53	0.40	0.40	0.40	3.2/10	8.0/10
RealMan	Dahuan	0.33	0.13	0.13	0.10	0.00	0.00	0.0/10	0.0/10

**TABLE V: Cross-Embodiment Evaluation Results under *Novel* Environment.** We further replace the background and the target objects following the same protocol as described in §IV-A.6. New hardware is highlighted in yellow.

venting them from maintaining their in-domain performance, CAGE consistently outperforms these baseline methods. Notably, in the ***Transport*** task with a football as the target, CAGE achieves an average success rate of 0.67 without any fine-tuning for this object, showcasing its potential to transfer manipulation skills to visually distinct objects.

3) *Unseen Environment*: For the  $L_2$  evaluations, we introduce distribution shifts on background, object, and camera view at the same time, resulting in the most challenging test environments. The results are illustrated in Tab. II.

**CAGE exhibits a strong generalization ability even to unseen environments, efficiently completing the task in out-of-domain situations without the need for fine-tuning.** CAGE remains an average of over 0.5 success rate while other policies still struggle to recognize the target object in the environment. This further demonstrates the effectiveness of our approach in learning manipulation-specific tasks while retaining most of the object-centric knowledge within the pre-trained visual encoders.

### C. Cross-Embodiment Evaluations

Apart from visual generalization capabilities, it is essential for a generalizable policy to effectively perform the learned tasks on new embodiments. Despite the inherent challenges, we report the task success rates for the ***Transport*** and ***Dumping*** tasks, as well as the completion rates for the latter, on new platforms with different hardware configurations.

The evaluation results on two similar platforms featuring either a new gripper or a different type of robotic arm are presented in Tab. IV and Tab. V. A significant performance drop is expected given the entirely new workspaces and manipulation interfaces. Nonetheless, for straightforward pick-and-place tasks like ***Transport***, CAGE achieves a near 50% success rate in most cases, except for configurations involving the RealMan arm in a *novel* environment.

Additionally, we observe that for more delicate tasks, our model demonstrates greater robustness to changes in the gripper compared to variations in the robotic arm. While these results do not yet meet the standard of excellence, we hope they can serve as a valuable baseline for future



Success Rate	CAGE (semi-in-domain)	CAGE (RH20T, out-of-box)
Reach	0.93	0.80 (-0.13)
Grasp	0.80	0.67 (-0.13)
Drop	0.73	0.67 (-0.06)

**TABLE VI: Results of the Out-of-Box Evaluation.** The figure on the left illustrates the out-of-box environments for CAGE pre-trained on RH20T [14]. Note that none of the object, background, and camera views appear in the training dataset.

efforts aimed at enhancing cross-embodiment generalization performance.

### D. RH20T Pre-training

In addition to the self-collected, high-quality dataset, we train CAGE on the same ***Transport*** task from RH20T [14] to evaluate the out-of-box generalization ability after pre-training. This dataset contains 164 demonstrations, collected by 14 operators under 4 different embodiments, and incorporates diverse distractors and rich variations in object sizes, backgrounds, and camera views. For evaluation, we design a blue cuboid<sup>2</sup> that differs from the training blocks both in texture and shape as the target. As illustrated in Tab. VI, we observe that while baselines fail to perform the task, **CAGE is capable of operating out-of-box and achieving comparable performance against being trained with a semi-in-domain high-quality dataset** (only same in the camera view). This proves that our approach can be scaled up to large and diverse datasets and yield a corresponding performance improvement.

### E. Ablations

1) *Model Components*: As shown in Tab. VII, we observe significant performance gains across the base and  $L_1$  levels of evaluations with the introduction of Causal Observation Perceiver (2nd row v.s. 3rd row). This validates our statements in §III that **Causal Observation Perceiver can**

<sup>2</sup>The originally purposed test object (football) is already used as a distractor in this dataset.

Ablation	L <sub>0</sub>			L <sub>1,bg</sub>			L <sub>1,obj</sub>			L <sub>1,cam</sub>		
	reach	grasp	drop	reach	grasp	drop	reach	grasp	drop	reach	grasp	drop
CAGE ( <i>ours</i> )	1.00	1.00	1.00	0.87	0.87	0.87	0.93	0.80	0.80	1.00	0.80	0.80
- Attn-UNet	0.80	0.80	0.80	0.80	0.67	0.67	0.73	0.73	0.73	0.80	0.67	0.67
- Causal Obs. Perceiver	0.47	0.40	0.40	0.40	0.13	0.13	0.27	0.00	0.00	0.40	0.20	0.20
- DINOv2 <sup>3</sup>	0.93	0.73	0.73	0.00	0.00	0.00	0.00	0.00	0.00	0.67	0.53	0.47
DP [6]	0.93	0.73	0.73	0.00	0.00	0.00	0.00	0.00	0.00	0.53	0.27	0.27

TABLE VII: Ablation Results in *Transport* Task. Three key components are sequentially removed from CAGE.

w/wo. Geo. Aug.	L <sub>1,cam</sub> (upper left)	L <sub>1,cam</sub> (lower right)	L <sub>2</sub>
	0.80	0.80	0.40
✓	<b>0.87</b>	<b>0.93</b>	<b>0.73</b>

TABLE VIII: Ablation Results *w/wo* Geometric Augmentations.

effectively retain both spatial and temporal information, facilitating the extraction of features for manipulation.

Interestingly, replacing the original ResNet [21] image encoder to DINOv2 [37] hinders the performance, supporting the claim that end-to-end training yields better in-domain performance [6, 36]. However, the model with DINOv2 shows improved ability to recognize targets with texture changes ( $L_{1,bg}$  and  $L_{1,obj}$ ), resulting in a higher success rate for reach (3rd row *v.s.* 4th row).

Moreover, the addition of attention modules also brings considerable improvements in all tests, with an average of more than 20% increase. This proves that **decoupling diffusion timestep with observation inputs and keeping the temporal relationship of history observations can help the policy learn generalizable manipulation skills**.

2) *Geometric Augmentation*: In our initial setup (§IV-A.7), we intentionally exclude random cropping and other augmentation methods, creating a mono-distributed training environment. We now unlock the full potential of CAGE by applying geometric augmentations, including random perspective transform followed by random cropping. The results shown in Tab. VIII demonstrate a significant boost in generalization abilities, notably with an 82.5% increase in success rate in the  $L_2$  evaluation. Therefore, for better performance in the challenging  $L_2$  evaluations, we include these geometric augmentations for all image-based policies.

3) *Observation Horizon*: Unlike DP [6], CAGE can handle long observation horizon from multiple cameras efficiently. We show the performance comparisons of the observation horizon  $T_o$  in Tab. IX, and find that  $T_o = 4$  performs better than the original DP implementation ( $T_o = 2$ ), demonstrating the superiority of our approach in effectively extracting and utilizing temporal information from a larger history window.

## V. CONCLUSION

In this work, we introduce CAGE, a data-efficient robotic manipulation policy that demonstrates strong generalization

<sup>3</sup>After removing DINOv2, the remaining model is still not identical to DP [6], as we opt for an observation horizon of 4 rather than 2 and use proprioception as the prefix to the noisy actions. Please refer to Appendix A for detailed explanations.

Observation Horizon $T_o$	Transport, L <sub>0</sub>		
	reach	grasp	drop
2	<b>1.00</b>	0.87	0.87
4	<b>1.00</b>	<b>1.00</b>	<b>1.00</b>
8	0.87	0.87	0.87

TABLE IX: Ablation Results of the Observation Horizon.

abilities in handling different levels of distribution shifts. We show that the success of CAGE is based on the collaboration of three key components: The vision foundation model as encoder, a causal observation perceiver, and an attention-augmented UNet as the action predictor. Through extensive experiments, CAGE not only outperforms DP [6], but also surpasses 3D-based RISE [54] by a considerable margin in terms of generalization. Despite CAGE’s success, we have observed several possible directions for future improvements. For example, in out-of-box evaluations, we find that CAGE performs better within the workspace of RH20T (7/8) than those positions outside (3/7), suggesting that data augmentations at the trajectory level might be needed for an enhanced workspace generalizability. Moreover, on the **Chopping** task, CAGE as well as baselines all fail to chop cleanly, resulting in connected pieces. After examination, we find that such difficulty also exists for human operators in the absence of force feedback from the haptic device. This highlights the necessity for the control policy to incorporate real-time force data for such contact-rich tasks.

## ACKNOWLEDGEMENT

We would like to thank Chenxi Wang for insightful discussions and for setting up the RealMan platform in cross-embodiment evaluations, Yiming Wang and Zihao He for their help during the data collection process.

## REFERENCES

- [1] Homanga Bharadhwaj et al. “RoboAgent: Generalization and Efficiency in Robot Manipulation via Semantic Augmentations and Action Chunking”. In: *IEEE International Conference on Robotics and Automation, ICRA 2024, Yokohama, Japan, May 13-17, 2024*. IEEE, 2024, pp. 4788–4795.
- [2] Anthony Brohan et al. “RT-1: Robotics Transformer for Real-World Control at Scale”. In: *Robotics: Science and Systems XIX, Daegu, Republic of Korea, July 10-14, 2023*. Ed. by Kostas E. Bekris et al. 2023.
- [3] Kaylee Burns et al. “What Makes Pre-Trained Visual Representations Successful for Robust Manipulation?” In: *arXiv preprint arXiv:2312.12444* (2023).

[4] Mathilde Caron et al. "Emerging Properties in Self-Supervised Vision Transformers". In: *2021 IEEE/CVF International Conference on Computer Vision, ICCV 2021, Montreal, QC, Canada, October 10-17, 2021*. IEEE, 2021, pp. 9630–9640.

[5] Xinlei Chen, Saining Xie, and Kaiming He. "An Empirical Study of Training Self-Supervised Vision Transformers". In: *2021 IEEE/CVF International Conference on Computer Vision, ICCV 2021, Montreal, QC, Canada, October 10-17, 2021*. IEEE, 2021, pp. 9620–9629.

[6] Cheng Chi et al. "Diffusion Policy: Visuomotor Policy Learning via Action Diffusion". In: *Robotics: Science and Systems XIX, Daegu, Republic of Korea, July 10-14, 2023*. Ed. by Kostas E. Bekris et al. 2023.

[7] Cheng Chi et al. "Universal Manipulation Interface: In-The-Wild Robot Teaching Without In-The-Wild Robots". In: *Proceedings of Robotics: Science and Systems (RSS)*. 2024.

[8] Open X-Embodiment Collaboration et al. "Open X-Embodiment: Robotic Learning Datasets and RT-X Models". In: *2024 IEEE International Conference on Robotics and Automation (ICRA)*. IEEE, 2024, pp. 6892–6903.

[9] Dahuan AG Series Gripper. Sept. 2024. URL: <https://en.dh-robotics.com/product/ag>.

[10] Dima Damen et al. "Rescaling Egocentric Vision: Collection, Pipeline and Challenges for EPIC-KITCHENS-100". In: *Int. J. Comput. Vis.* 130.1 (2022), pp. 33–55.

[11] Norman Di Palo and Edward Johns. "Keypoint Action Tokens Enable In-Context Imitation Learning in Robotics". In: *arXiv preprint arXiv:2403.19578* (2024).

[12] Alexey Dosovitskiy et al. "An Image is Worth 16x16 Words: Transformers for Image Recognition at Scale". In: *9th International Conference on Learning Representations, ICLR 2021, Virtual Event, Austria, May 3-7, 2021*. OpenReview.net, 2021.

[13] Haoshu Fang et al. "AnyGrasp: Robust and Efficient Grasp Perception in Spatial and Temporal Domains". In: *IEEE Trans. Robotics* 39.5 (2023), pp. 3929–3945.

[14] Haoshu Fang et al. "RH20T: A Comprehensive Robotic Dataset for Learning Diverse Skills in One-Shot". In: *IEEE International Conference on Robotics and Automation, ICRA 2024, Yokohama, Japan, May 13-17, 2024*. IEEE, 2024, pp. 653–660.

[15] Flexiv Rizon Robot. Sept. 2024. URL: <https://www.flexiv.com/product/rizon>.

[16] Force Dimension - sigma.7. Sept. 2024. URL: <https://www.forcedimension.com/products/sigma>.

[17] Théophile Gervet et al. "Act3D: 3D Feature Field Transformers for Multi-Task Robotic Manipulation". In: *Conference on Robot Learning, CoRL 2023, 6-9 November 2023, Atlanta, GA, USA*. Ed. by Jie Tan, Marc Toussaint, and Kouroush Darvish. Vol. 229. Proceedings of Machine Learning Research. PMLR, 2023, pp. 3949–3965.

[18] Raghav Goyal et al. "The "Something Something" Video Database for Learning and Evaluating Visual Common Sense". In: *IEEE International Conference on Computer Vision, ICCV 2017, Venice, Italy, October 22-29, 2017*. IEEE Computer Society, 2017, pp. 5843–5851.

[19] Kristen Grauman et al. "Ego4D: Around the World in 3,000 Hours of Egocentric Video". In: *IEEE/CVF Conference on Computer Vision and Pattern Recognition, CVPR 2022, New Orleans, LA, USA, June 18-24, 2022*. IEEE, 2022, pp. 18973–18990.

[20] Jean-Bastien Grill et al. "Bootstrap Your Own Latent - A New Approach to Self-Supervised Learning". In: *Advances in Neural Information Processing Systems 33: Annual Conference on Neural Information Processing Systems 2020, NeurIPS 2020, December 6-12, 2020, virtual*. Ed. by Hugo Larochelle et al. 2020.

[21] Kaiming He et al. "Deep Residual Learning for Image Recognition". In: *2016 IEEE Conference on Computer Vision and Pattern Recognition, CVPR 2016, Las Vegas, NV, USA, June 27-30, 2016*. IEEE Computer Society, 2016, pp. 770–778.

[22] Kaiming He et al. "Masked Autoencoders Are Scalable Vision Learners". In: *IEEE/CVF Conference on Computer Vision and Pattern Recognition, CVPR 2022, New Orleans, LA, USA, June 18-24, 2022*. IEEE, 2022, pp. 15979–15988.

[23] Edward J. Hu et al. "LoRA: Low-Rank Adaptation of Large Language Models". In: *The Tenth International Conference on Learning Representations, ICLR 2022, Virtual Event, April 25-29, 2022*. OpenReview.net, 2022.

[24] Intel RealSense Depth Camera D415. Sept. 2024. URL: <https://www.intelrealsense.com/depth-camera-d415>.

[25] Intel RealSense Depth Camera D435. Sept. 2024. URL: <https://www.intelrealsense.com/depth-camera-d435>.

[26] Andrew Jaegle et al. "Perceiver IO: A General Architecture for Structured Inputs & Outputs". In: *The Tenth International Conference on Learning Representations, ICLR 2022, Virtual Event, April 25-29, 2022*. OpenReview.net, 2022.

[27] Alexander Khazatsky et al. "Droid: A large-scale in-the-wild robot manipulation dataset". In: *arXiv preprint arXiv:2403.12945* (2024).

[28] Moo Jin Kim et al. "OpenVLA: An Open-Source Vision-Language-Action Model". In: *arXiv preprint arXiv:2406.09246* (2024).

[29] Alexander Kirillov et al. "Segment Anything". In: *IEEE/CVF International Conference on Computer Vision, ICCV 2023, Paris, France, October 1-6, 2023*. IEEE, 2023, pp. 3992–4003.

[30] Xingyu Lin et al. "SpawnNet: Learning Generalizable Visuomotor Skills from Pre-trained Network". In: *IEEE International Conference on Robotics and Automation, ICRA 2024, Yokohama, Japan, May 13-17, 2024*. IEEE, 2024, pp. 4781–4787.

[31] Zeyi Liu et al. "ManiWAV: Learning Robot Manipulation from In-the-Wild Audio-Visual Data". In: *arXiv preprint arXiv:2406.19464* (2024).

[32] Yecheng Jason Ma et al. "LIV: Language-Image Representations and Rewards for Robotic Control". In: *International Conference on Machine Learning, ICML 2023, 23-29 July 2023, Honolulu, Hawaii, USA*. Ed. by Andreas Krause et al. Vol. 202. Proceedings of Machine Learning Research. PMLR, 2023, pp. 23301–23320.

[33] Arjun Majumdar et al. "Where are we in the search for an Artificial Visual Cortex for Embodied Intelligence?" In: *Advances in Neural Information Processing Systems 36: Annual Conference on Neural Information Processing Systems 2023, NeurIPS 2023, New Orleans, LA, USA, December 10 - 16, 2023*. Ed. by Alice Oh et al. 2023.

[34] Ajay Mandlekar et al. "What Matters in Learning from Offline Human Demonstrations for Robot Manipulation". In: *Conference on Robot Learning, 8-11 November 2021, London, UK*. Ed. by Aleksandra Faust, David Hsu, and Gerhard Neumann. Vol. 164. Proceedings of Machine Learning Research. PMLR, 2021, pp. 1678–1690.

[35] Suraj Nair et al. "R3M: A Universal Visual Representation for Robot Manipulation". In: *Conference on Robot Learning, CoRL 2022, 14-18 December 2022, Auckland, New Zealand*. Ed. by Karen Liu, Dana Kulic, and Jeffrey Ichniowski. Vol. 205. Proceedings of Machine Learning Research. PMLR, 2022, pp. 892–909.

[36] Octo Model Team et al. "Octo: An Open-Source Generalist Robot Policy". In: *Proceedings of Robotics: Science and Systems (RSS)*. 2024.

[37] Maxime Oquab et al. “DINOv2: Learning Robust Visual Features without Supervision”. In: *Trans. Mach. Learn. Res.* 2024 (2024).

[38] Jyothish Pari et al. “The Surprising Effectiveness of Representation Learning for Visual Imitation”. In: *Robotics: Science and Systems XVIII, New York City, NY, USA, June 27 - July 1, 2022*. Ed. by Kris Hauser, Dylan A. Shell, and Shoudong Huang. 2022.

[39] Ethan Perez et al. “FiLM: Visual Reasoning with a General Conditioning Layer”. In: *Proceedings of the Thirty-Second AAAI Conference on Artificial Intelligence, (AAAI-18), the 30th innovative Applications of Artificial Intelligence (IAAI-18), and the 8th AAAI Symposium on Educational Advances in Artificial Intelligence (EAAI-18), New Orleans, Louisiana, USA, February 2-7, 2018*. Ed. by Sheila A. McIlraith and Kilian Q. Weinberger. AAAI Press, 2018, pp. 3942–3951.

[40] Dean Pomerleau. “ALVINN: An Autonomous Land Vehicle in a Neural Network”. In: *Advances in Neural Information Processing Systems 1, [NIPS Conference, Denver, Colorado, USA, 1988]*. Ed. by David S. Touretzky. Morgan Kaufmann, 1988, pp. 305–313.

[41] Jianing Qian, Anastasios Panagopoulos, and Dinesh Jayaraman. “Recasting Generic Pretrained Vision Transformers As Object-Centric Scene Encoders For Manipulation Policies”. In: *IEEE International Conference on Robotics and Automation, ICRA 2024, Yokohama, Japan, May 13-17, 2024*. IEEE, 2024, pp. 17544–17552.

[42] Alec Radford et al. “Learning Transferable Visual Models From Natural Language Supervision”. In: *Proceedings of the 38th International Conference on Machine Learning, ICML 2021, 18-24 July 2021, Virtual Event*. Ed. by Marina Meila and Tong Zhang. Vol. 139. Proceedings of Machine Learning Research. PMLR, 2021, pp. 8748–8763.

[43] Ilija Radosavovic et al. “Real-World Robot Learning with Masked Visual Pre-training”. In: *Conference on Robot Learning, CoRL 2022, 14-18 December 2022, Auckland, New Zealand*. Ed. by Karen Liu, Dana Kulic, and Jeffrey Ichnowski. Vol. 205. Proceedings of Machine Learning Research. PMLR, 2022, pp. 416–426.

[44] Robin Rombach et al. “High-Resolution Image Synthesis with Latent Diffusion Models”. In: *IEEE/CVF Conference on Computer Vision and Pattern Recognition, CVPR 2022, New Orleans, LA, USA, June 18-24, 2022*. IEEE, 2022, pp. 10674–10685.

[45] Olaf Ronneberger, Philipp Fischer, and Thomas Brox. “U-Net: Convolutional Networks for Biomedical Image Segmentation”. In: *Medical Image Computing and Computer-Assisted Intervention - MICCAI 2015 - 18th International Conference Munich, Germany, October 5 - 9, 2015, Proceedings, Part III*. Ed. by Nassir Navab et al. Vol. 9351. Lecture Notes in Computer Science. Springer, 2015, pp. 234–241.

[46] Dandan Shan et al. “Understanding Human Hands in Contact at Internet Scale”. In: *2020 IEEE/CVF Conference on Computer Vision and Pattern Recognition, CVPR 2020, Seattle, WA, USA, June 13-19, 2020*. Computer Vision Foundation / IEEE, 2020, pp. 9866–9875.

[47] Jinghuan Shang et al. “Theia: Distilling Diverse Vision Foundation Models for Robot Learning”. In: *arXiv preprint arXiv:2407.20179* (2024).

[48] Mohit Shridhar, Lucas Manuelli, and Dieter Fox. “Perceiver-Actor: A Multi-Task Transformer for Robotic Manipulation”. In: *Conference on Robot Learning, CoRL 2022, 14-18 December 2022, Auckland, New Zealand*. Ed. by Karen Liu, Dana Kulic, and Jeffrey Ichnowski. Vol. 205. Proceedings of Machine Learning Research. PMLR, 2022, pp. 785–799.

[49] Jiaming Song, Chenlin Meng, and Stefano Ermon. “De-noising Diffusion Implicit Models”. In: *9th International Conference on Learning Representations, ICLR 2021, Virtual Event, Austria, May 3-7, 2021*. OpenReview.net, 2021.

[50] Ashish Vaswani et al. “Attention is All you Need”. In: *Advances in Neural Information Processing Systems 30: Annual Conference on Neural Information Processing Systems 2017, December 4-9, 2017, Long Beach, CA, USA*. Ed. by Isabelle Guyon et al. 2017, pp. 5998–6008.

[51] Homer Rich Walke et al. “BridgeData V2: A Dataset for Robot Learning at Scale”. In: *Conference on Robot Learning, CoRL 2023, 6-9 November 2023, Atlanta, GA, USA*. Ed. by Jie Tan, Marc Toussaint, and Kourosh Darvish. Vol. 229. Proceedings of Machine Learning Research. PMLR, 2023, pp. 1723–1736.

[52] Weikang Wan et al. “UniDexGrasp++: Improving Dexterous Grasping Policy Learning via Geometry-aware Curriculum and Iterative Generalist-Specialist Learning”. In: *IEEE/CVF International Conference on Computer Vision, ICCV 2023, Paris, France, October 1-6, 2023*. IEEE, 2023, pp. 3868–3879.

[53] Chen Wang et al. “DexCap: Scalable and Portable Mocap Data Collection System for Dexterous Manipulation”. In: *arXiv preprint arXiv:2403.07788* (2024).

[54] Chenxi Wang et al. “RISE: 3D Perception Makes Real-World Robot Imitation Simple and Effective”. In: *arXiv preprint arXiv:2404.12281* (2024).

[55] Yanjie Ze et al. “3D Diffusion Policy: Generalizable Visuomotor Policy Learning via Simple 3D Representations”. In: *Proceedings of Robotics: Science and Systems (RSS)*. 2024.

[56] Yanjie Ze et al. “GNFactor: Multi-Task Real Robot Learning with Generalizable Neural Feature Fields”. In: *Conference on Robot Learning, CoRL 2023, 6-9 November 2023, Atlanta, GA, USA*. Ed. by Jie Tan, Marc Toussaint, and Kourosh Darvish. Vol. 229. Proceedings of Machine Learning Research. PMLR, 2023, pp. 284–301.

[57] Junjie Zhang et al. “SAM-E: Leveraging Visual Foundation Model with Sequence Imitation for Embodied Manipulation”. In: *Forty-first International Conference on Machine Learning, ICML 2024, Vienna, Austria, July 21-27, 2024*. OpenReview.net, 2024.

[58] Tong Zhang et al. “A Universal Semantic-Geometric Representation for Robotic Manipulation”. In: *Conference on Robot Learning, CoRL 2023, 6-9 November 2023, Atlanta, GA, USA*. Ed. by Jie Tan, Marc Toussaint, and Kourosh Darvish. Vol. 229. Proceedings of Machine Learning Research. PMLR, 2023, pp. 3342–3363.

[59] Tony Z. Zhao et al. “Learning Fine-Grained Bimanual Manipulation with Low-Cost Hardware”. In: *Robotics: Science and Systems XIX, Daegu, Republic of Korea, July 10-14, 2023*. Ed. by Kostas E. Bekris et al. 2023.

[60] Brianna Zitkovich et al. “RT-2: Vision-Language-Action Models Transfer Web Knowledge to Robotic Control”. In: *Conference on Robot Learning, CoRL 2023, 6-9 November 2023, Atlanta, GA, USA*. Ed. by Jie Tan, Marc Toussaint, and Kourosh Darvish. Vol. 229. Proceedings of Machine Learning Research. PMLR, 2023, pp. 2165–2183.

### A. Implementation Details

We provide detailed information about the architecture of CAGE and our implementations of the selected baselines DP [6] and RISE [54]. Main hyper-parameters used for training and evaluation are presented in Tab. X for comparison.

1) *CAGE*: Our model uses DINOv2-large [37] as the vision encoder backbone. In order to preserve its rich semantic knowledge learned from pre-training, the weights of DINOv2 are kept frozen and we employ LoRA [23] on the projector matrices of the attention modules for parameter-efficient fine-tuning. LoRA rank is set to 16 and a dropout rate of 0.1 is applied to avoid over-fitting. We set the observation horizon  $T_o = 4$  based on the ablation results (Tab. IX in §IV-E). The images are first resized to  $256 \times 256$  and then cropped to  $224 \times 224$  as observation inputs. The vision encoder outputs  $L = 256$  tokens of dimension  $D = 1024$  for each frame. These tokens are first projected into  $D_{\text{token}} = 512$ . Then,  $N_c \times T_o \times L = 2 \times 4 \times 256 = 2048$  tokens are compressed into  $T_o = 4$  tokens via our proposed *Causal Observation Perceiver*. The perceiver is composed of a cross-attention module followed by self-attention modules with causal masks:  $T_o$  learnable tokens are cross-attended to concatenated observation tokens using a causal mask for each camera; the output tokens are then passed into a sequence of  $N = 4$  causal self-attention modules for further processing. Dropout layers with  $p = 0.1$  are also applied on each attention block for a more robust feature extraction. Modified from the pure CNN-based noise prediction network [6], we append a *Cross-Attention Block* to each *Residual Block* for separate conditioning of observation and timestep. We adopt the default setting of a 3-layer UNet with increased channel dimensions 256-512-1024 as suggested in [6]. For the data augmentation, only the color jitter is included in  $L_0$  and  $L_1$  generalization evaluations, and additional geometric augmentation (§IV-E) is applied in  $L_2$  evaluations for better overall performance.

2) *DP*: The CNN-based Diffusion Policy is implemented following the official implementation, except that the vision encoder is upgraded from ResNet-18 to ResNet-50 for a higher capacity in visual expressiveness. Given that DP performs better with a shorter observation horizon, we keep  $T_o = 2$  and  $T_a = 16$ . All other hyper-parameters are aligned with those of CAGE to facilitate direct comparisons. The augmentations also follows the CAGE implementations. Moreover, a strictly aligned  $T_o = 4$  and  $T_a = 20$  version of DP is included in Tab. VII (4th row) for the ablation study.

3) *Rise*: The configuration of RISE remains the same as the official implementation, except that we enable the color jitter augmentation option during training for fair generalization comparisons. Following their original settings, RISE only takes the point cloud from a single fixed camera with observation horizon  $T_o = 1$  as inputs, and outputs continuous actions for  $T_a = 20$  steps. RISE adopts absolute action representations in the camera coordinate.

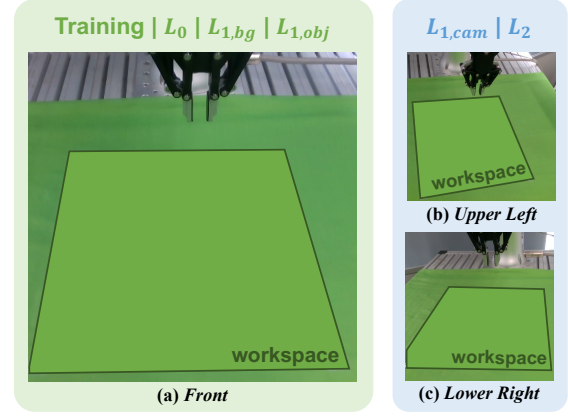


**Fig. 4: Observation Images from Different Cameras.** The front camera is used as the fixed camera for training and camera-in-domain experiments ( $L_0$ ,  $L_{1,bg}$  and  $L_{1,obj}$ ). The upper-left and lower-right cameras are utilized for camera-out-of-domain generalization experiments ( $L_{1,cam}$  and  $L_2$ ). Both alternative viewpoints introduce a considerable amount of visual distortion.

### B. Task Details

We design three types of tasks, each corresponding to a different aspect of the robotic manipulation problem.

- **Pick-and-place task**: The pick-and-place task represents the most fundamental and widely utilized operation in robotic control. The *Transport* task (samples shown in Fig. 6) consists of the robotic arm first picking up the object on the left half of the workspace and dropping it to the right. This task necessitates the robot's capacity to accurately locate and reach the target object, precisely grasp it with an appropriate pose, and drop it in the designated location. *We use the Transport task to assess the policy's generalization ability for the elementary skills.*
- **6-DoF task**: By unlocking two more degrees of freedom in rotation, 6-DoF actions can greatly facilitate the robot's interaction with objects. The *Dumping* task (samples shown in Fig. 7) can be decomposed into 3 sub-tasks with rotations: grasp the plastic cup horizontally; move it over the bowl and pour all 10 balls into the bowl; place the cup vertically inside the target area. During the prediction, the policy must determine if additional rotation is required based on the observation inputs. This presents a significant challenge for the model in terms of understanding its own state within the environment. *We design the Dumping task to test whether the policy can understand its own state within the environment and produce coherent rotations against visual variations.*
- **Long-horizon task**: In many scenarios, a single task is composed of several repetitive small tasks that often have to be executed in order. This underscores the robustness and flexibility of the policy during the interaction with the environment. The objective of the *Chopping* task (samples shown in Fig. 8) is to grasp properly the kitchen knife, chop the pepper on the cutting board into several pieces, and place the knife

	CAGE ( <i>ours</i> )	DP [6]	RISE [54]
Observation Horizon $T_o$	4	2	1
Action Horizon $T_a$	20	16	20
Proprioception	✓	✗	✗
Camera Setting	1 fixed + 1 in-hand	1 fixed + 1 in-hand	1 fixed
Observation Type	RGB	RGB	RGB-D
Observation Resolution	$224 \times 224$ (image)	$224 \times 224$ (image)	$1280 \times 720$ (point cloud)
Vision Encoder	DINOv2-large  w. LoRA	ResNet-50	Sparse 3D Encoder
Observation Perceiver	✓	✗	✗
UNet of Diffusion Head	3 layers (256-512-1024)	3 layers (256-512-1024)	2 layers (256-512)
Denoising Steps	16	16	16
Inference Time	280ms	100ms	130ms
Temporal Ensemble [59]	✓ (first 12 steps)	✓ (first 12 steps)	✓ (all $T_a$ steps)
Control Type	parallel	parallel	blocking
Control Frequency	10Hz	10Hz	✗
Prediction Frequency	every 0.35s	every 0.35s	every 4 steps

TABLE X: Detailed Comparison of All Policies. / denotes frozen/trainable weights respectively.

safely on the foam pad. The robotic arm is required to conduct multiple chopping evenly and progressively. We employ the **Chopping** task to evaluate the task planning and error recovery abilities of the model in out-of-distribution scenes.

### C. Evaluation Details

In order to evaluate the generalization performance of each policy, we devise distribution shifts on three principal visual factors that are particularly susceptible to variation upon deployment in the real world:

- **Background:** The original green background is changed to a white leather-textured one or a tablecloth with light and dark geometric patterns depending on the task.
- **Object:** We modify the target object’s color and geometry to evaluate the object-level generalizability of manipulation policies. For the **Dumping** and the **Chopping** tasks, in addition to the change of the target object (bowl in **Dumping** and pepper in **Chopping**), we also alter the color of the cardboard (in **Dumping**) or the foam pad (in **Chopping**). In the **Transport** task, we additionally test the policies using a football, which poses a serious challenge due to the huge difference in geometry and the need for strong self-correction skills following unsuccessful attempts.
- **Camera View:** We introduce a large visual distortions by displacing the camera approximately 16cm away from the original position. Additionally, the original fixed Intel RealSense D435 camera [25] is replaced with an Intel RealSense D415 camera [24] for a more challenging setup. The images from different cameras are shown in Fig. 4, from which we can observe a significant view discrepancy between training and evaluation cameras.

Therefore, we define three levels of generalization tests:

- **L<sub>0</sub> generalization** is conducted in the same environment seen during training. We evaluate the most basic

ability of the policy to learn the task from demonstrations.

- **L<sub>1</sub> generalization** is conducted in a similar environment with the variation in one of the three visual aspects, which we refer to as  $L_{1,bg}$ ,  $L_{1,obj}$  and  $L_{1,cam}$  respectively. We evaluate the robustness of the policy under moderate distribution shifts.
- **L<sub>2</sub> generalization** is conducted in a totally unseen environment with variations on all three aspects. We evaluate the capability of the policy to complete the learned task in out-of-domain scenes.

Moreover, we use a script<sup>4</sup> to generate randomly and uniformly distributed evaluation positions *beforehand* for each task, ensuring a fair, consistent, and reproducible comparison across different models under the same test, as shown in Fig. 5 for the example of the **Transport** task.

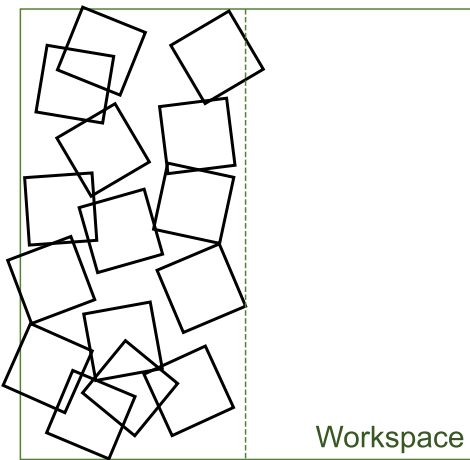
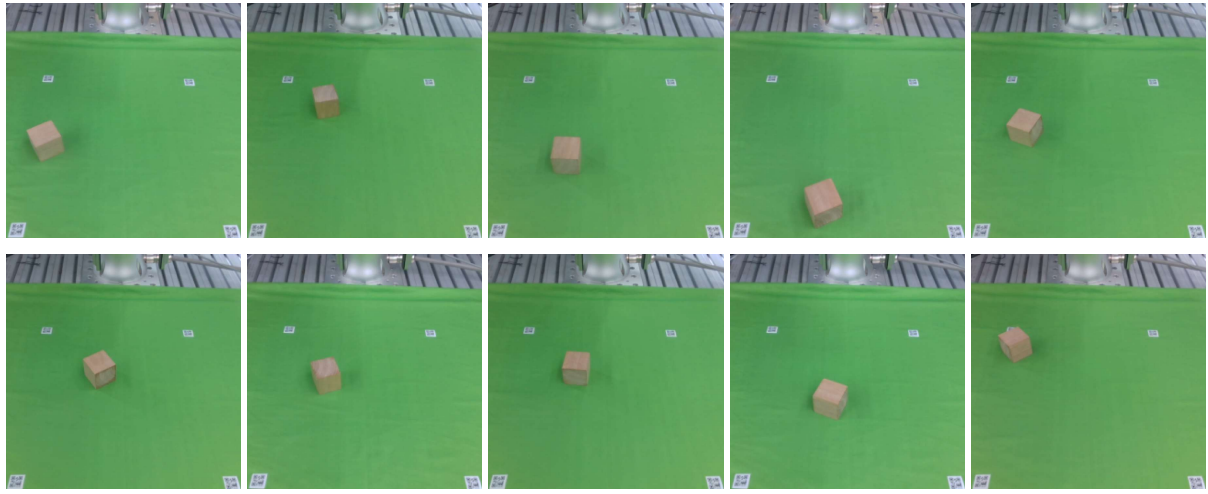
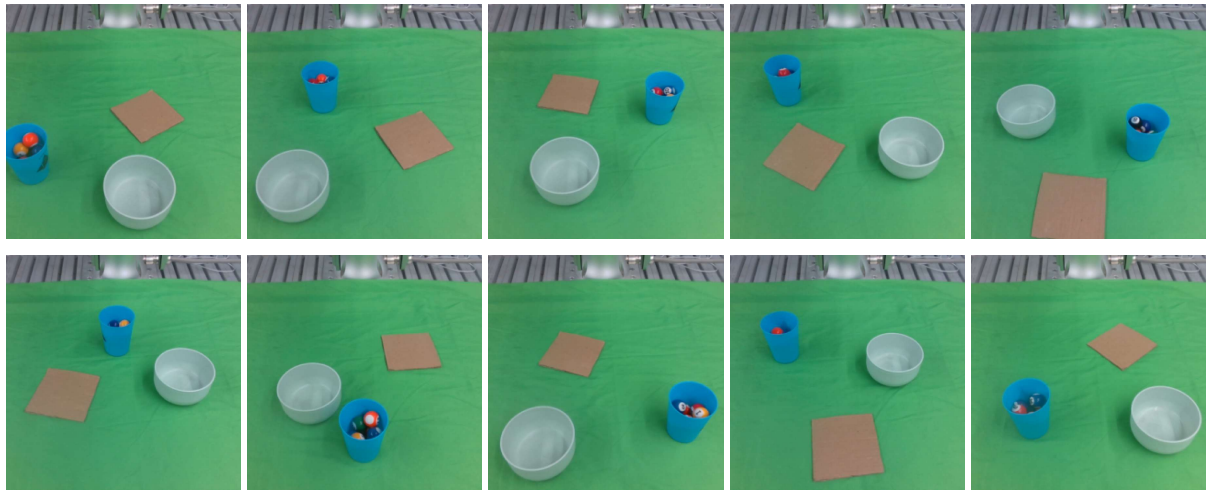


Fig. 5: Evaluation Initialization for the **Transport** Task. The target block is placed at each designated location for each evaluation round.

<sup>4</sup>The script for generating random initial object positions is also provided in our code repository.



**Fig. 6: Sample Initializations of the *Transport* Task.** The block is randomly initialized on the left part of the workspace.



**Fig. 7: Sample Initializations of the *Dumping* Task.** The cup (with 10 balls in it), the bowl, and the cardboard as the placement target area are randomly initialized on the workspace.



**Fig. 8: Sample Initializations of the *Chopping* Task.** A kitchen knife (with its base), a cutting board (with chili pepper on it), and a foam pad used for placement are randomly initialized on the workspace.